RESEARCH ARTICLE

Investigation of the mechanical and thermo- electrical properties of nylon filaments reinforced with nanoparticle

Farshad Farahbod[1], Abuzar Shakeri[2], Seyede Nasrin Hosseinimotlagh[3]*

[1] *Department of Chemical Engineering, Fir.C., Islamic Azad University, Firoozabad, Iran*

[2,3] *Department of Physics, Shi.C., Islamic Azad University, Shiraz, Iran*

ARTICLE INFO

Article History:

Received 2024-12-13
Accepted 2025s-04-11
Published 2024-02-15

Keywords:

Thermal properties,

Stress properties,

Nylon,

ZnO nano particles.

ABSTRACT

Incorporating zinc oxide nanoparticles (ZnONPs) into nylon significantly alters its mechanical and thermal characteristics. Nanocomposites with 0, 1, and 2 wt% ZnONPs were created through a two-step process of dry mixing and single-screw extrusion. Tensile testing (at strain rates from 0.02 to 2) showed that both neat nylon and the nanocomposites exhibit strain rate hardening, with ultimate tensile strength (UTS), yield strength, and tensile modulus all influenced by strain rate. Critically, adding ZnONPs improved these mechanical properties, with the 2 wt% nanocomposite showing a 45% higher tensile modulus and a 26% higher UTS than neat nylon. Thermal stability was enhanced by the nanoparticles, as confirmed by thermogravimetric analysis (TGA), and differential scanning calorimetry (DSC) revealed a slight increase in glass transition temperature. A constitutive model effectively captured the nonlinear, strain rate-dependent behavior of both the base polymer and the nanocomposites. While thermal conductivity and diffusivity showed complex trends with increasing ZnONP content, the 2 wt% sample exhibited the highest conductivity and lowest diffusivity. Finally, the dielectric constant increased, and resistivity decreased, with higher ZnONP loadings.

How to cite this article
Farahbod F., Shakeri A., Hosseinimotlagh S. N., Investigation of the mechanical and thermo- electrical properties of nylon filaments reinforced with nanoparticle. J. Nanoanalysis., 2024; 11(1): 662-667.

INTRODUCTION

Nylon 6, a versatile engineering thermoplastic, finds broad application due to its favorable combination of mechanical properties and chemical resistance [1]. However, conventional reinforcement strategies often require substantial filler content to achieve notable property enhancements, which can compromise the inherent advantages of the polymer [2]. Nanocomposites, leveraging small

*Corresponding Author Email: *Farshad.Farahbod@iau.ac.ir*

amounts of nanoparticles, offer a compelling alternative [3]. Zinc oxide nanoparticles (ZnONPs) are particularly attractive for reinforcing polymers due to their potential to improve mechanical performance [4]. This research investigates how incorporating ZnONPs affects the mechanical and thermal properties of nylon filaments [5]. Mechanical behavior is assessed through tensile testing, while Scanning Electron Microscopy (SEM) is employed to examine fracture surfaces and understand failure mechanisms [6]. Finally, experimental data informs the development of a constitutive model that describes the tensile behavior of the resulting nylon-ZnO nanocomposites [7]. Nanoparticle reinforcement offers a powerful method to tailor and enhance the properties of nylon fibers [8]. The following summarizes the primary impacts of incorporating nanoparticles into this material:

Incorporating nanoparticles into nylon fibers offers a pathway to significantly tailor and improve material performance [9]. These reinforcements impact mechanical, thermal, and other functional characteristics [10]. Mechanically, nanoparticles can increase strength and stiffness by acting as reinforcing agents within the nylon matrix, leading to improvements in tensile strength, yield strength, and modulus [11]. Some nanoparticles also enhance toughness, improving resistance to cracking and fracture, and reduce creep by hindering polymer chain movement under sustained stress [12]. Thermally, certain nanoparticles can improve thermal stability, increasing resistance to high-temperature degradation, and elevate the glass transition temperature (Tg), allowing the material to maintain stiffness and strength at higher temperatures [13]. Beyond these, nanoparticles can impart additional functionalities [14]. For example, titanium dioxide (TiO_2) or zinc oxide (ZnO) can provide UV protection, while silver nanoparticles (AgNPs) can introduce antimicrobial properties. Conductive nanoparticles, like carbon nanotubes or graphene, can even render nylon fibers electrically conductive. The degree of property modification is influenced by several key factors: the specific type of nanoparticle used, its concentration within the nylon matrix, the uniformity of nanoparticle dispersion (agglomeration can create weaknesses), and the processing technique employed (e.g., melt mixing, solution blending, or in-situ polymerization) [15]. This study focuses specifically on the tensile mechanical properties of nylon filaments reinforced with zinc oxide nanoparticles.

EXPERIMENTAL

Determining the novelty of a manuscript concerning the mechanical and tensile properties of nanoparticle-reinforced nylon filaments requires a thorough literature review. However, several potential areas of innovation can distinguish such work. These include developing a novel nanoparticle incorporation method (e.g., unique surface treatment, mixing/extrusion technique, or functionalization for enhanced nylon interaction), exploring less common nanoparticle types or combinations (with strong justification and investigation of synergistic effects), or focusing on a specific, under-studied mechanical property (e.g., fatigue, impact, creep, or wear) with detailed analysis as a function of concentration and processing. Critically, going beyond simply reporting property improvements and establishing detailed structure-property relationships via advanced characterization (e.g., TEM, SAXS) to analyze nanoparticle dispersion, interfacial bonding, and microstructural changes is essential for demonstrating originality. Other avenues for innovation include developing new theoretical models or employing advanced simulations (e.g., nanoscale finite element analysis) to understand deformation mechanisms, systematically optimizing processing parameters (e.g., extrusion temperature, screw speed, drawing ratio) using a design of experiments approach, or focusing on

a specific application and demonstrating how nanoparticle incorporation enhances performance in that context. Ultimately, manuscript originality hinges on demonstrating something new and non-obvious in the materials, processing, characterization, modeling, or application, with a clear articulation of the research gap and the work's contribution.

ZnONP Characterization

Zinc oxide nanoparticles (ZnONPs) exhibited a hexagonal wurtzite structure (Figure 1). As a semiconductor with a bandgap of approximately 3.22 eV, ZnO interacts with UV-visible light through electronic excitation between its conduction and valence bands, a phenomenon observed in other ZnO-containing materials as well [32, 33]. While ZnONPs have been shown to exhibit some agglomeration within material matrices, this study also investigated the impact of ZnO addition on the mechanical and optical properties of LDPE thin films. Young's modulus, strength, and elongation at break were determined from stress-strain curves. The presence of ZnO significantly altered these properties. The improved strain at fracture, regardless of ZnO concentration, suggests a mechanism involving surface adhesion and interaction between the ZnONPs and the LDPE matrix [33].

Materials

High-purity, sub-50 nm spherical zinc oxide nanoparticles (ZnONPs) were synthesized via a sol-gel method. The matrix material was a high-performance polyamide. 6 resins (Nylon P1011F) specifically designed for stable high-speed extrusion. This resin, according to supplier specifications, has a melting temperature range of 215-225 °C, a density of 1.09-1.19 g/cm³, and typical mechanical properties including 70-80 MPa tensile strength, 100% tensile elongation at break, and 1-3 GPa tensile modulus.

Research process

Nylon powder and precisely weighed ZnONPs were dry-mixed for one hour using a high-speed mechanical blender (22,000 rpm), with 10-minute cooling intervals to prevent thermal degradation. A single-screw extruder (19 mm screw diameter, five heating zones) melted and mixed the nylon and ZnONPs. The barrel temperature profile consisted of three progressively increasing zones (222 °C, 232 °C, and 242 °C) followed by two zones at 242 °C near the die, ensuring gradual melting and effective mixing. The homogenized nylon-ZnO nanocomposite was then extruded through a die plate, heated steel tube, and die (Figure 2).

Composite filaments were produced via continuous extrusion under controlled tension. The extruded material then passed through a godet wheel and heating zone before being wound onto a rotating bobbin at 70 rpm (Figure 3).

Testing

A START data acquisition system was used for all experiments. Three sample groups were analyzed: neat nylon filaments, and composite filaments with 1 wt% and 2 wt% ZnO nanoparticles. At least ten replicates per group were tested for statistical significance. FE-SEM samples were sectioned and argon plasma etched (TEK Vac Industries, Inc.) for one hour at 600 mTorr and 2.5 W/cm² power density.

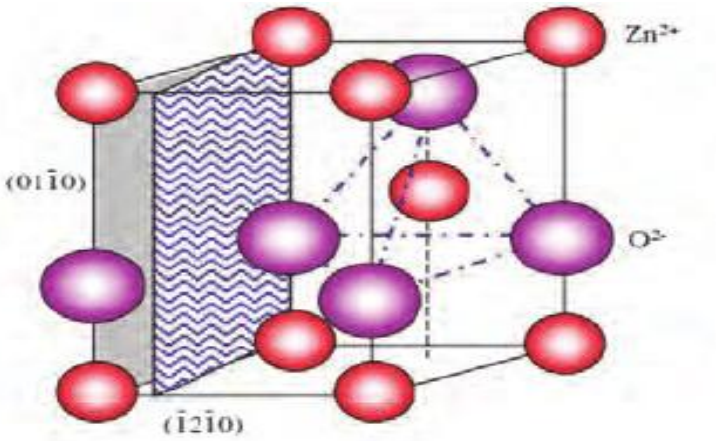

Figure 1. The wurtzite structure model of ZnO.

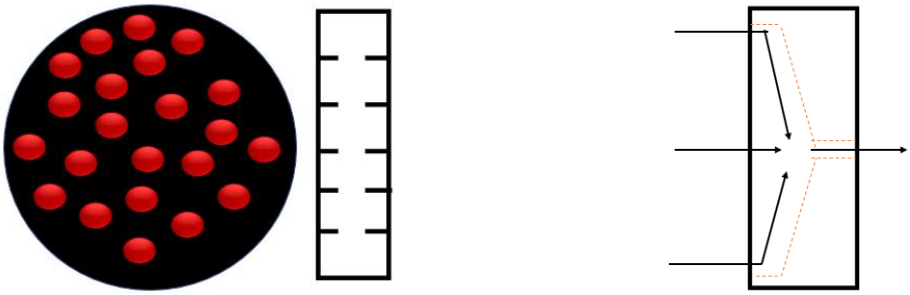

(a). (b).

Figure 2. Extruder die geometry. (a) Top view of circular die plate. (b) Side view of die profile.

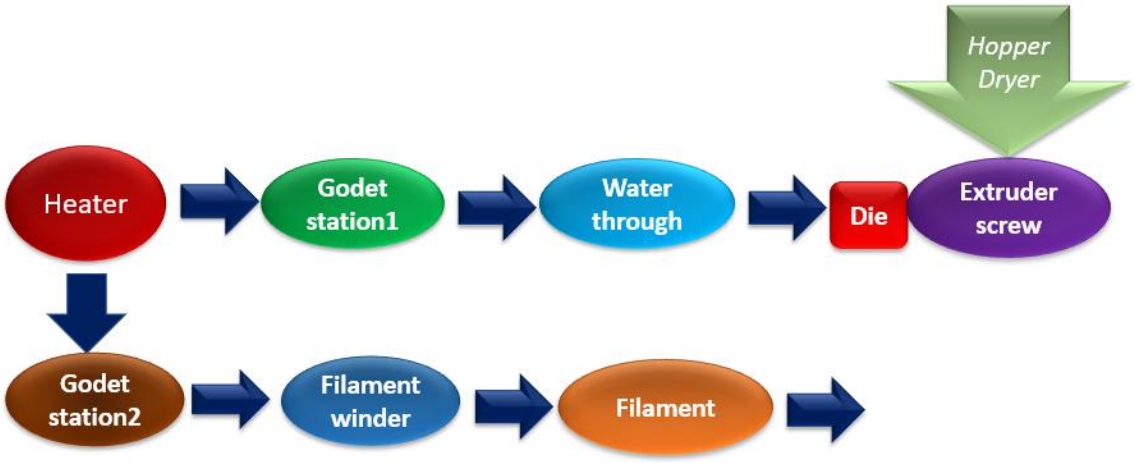

Figure 3. Schematic of the PAN-based carbon fiber spinning process.

RESULTS AND DISCUSSIONS

Thermal response

Thermogravimetric analysis (TGA) curves, shown in Figure 4a, depict the mass loss of neat nylon filaments and composite filaments with 1 wt% and 2 wt% ZnONP loadings as a function of temperature. Derivative thermogravimetric (DTG) curves (Figure 4b) were analyzed to determine the decomposition temperature. These curves, representing the rate of mass loss versus temperature, show peaks corresponding to the maximum degradation rates.

Derivative thermogravimetric (DTG) analysis (Figure 5b) revealed decomposition temperatures of 445°C for neat nylon, increasing to 455°C and 456°C with the addition of 1 wt% and 2 wt% ZnO nanoparticles, respectively. The glass transition temperature (Tg) (Figure 5a) also increased, from 49°C for neat nylon to 55°C and 56°C for the 1 wt% and 2 wt% nanocomposites, respectively. This elevation in Tg indicates that the incorporation of ZnO nanoparticles restricts the movement of nylon polymer chain segments.

Figure 5b shows that both 1 wt% and 2 wt% ZnO-nylon composites exhibit a higher crystallization temperature (Tc) of 193°C compared to 190°C for the neat nylon control. Crystallinity also increased from approximately 24% in the neat nylon to around 28% in both nanocomposites. These results indicate that the incorporated ZnO nanoparticles act as nucleating agents, promoting earlier crystallization and a higher degree of crystallinity. However, it is possible that higher nanoparticle concentrations could alter crystallization kinetics and potentially slow down the crystallization rate.

While the melting temperature (Tm) remained consistent at approximately 224°C across all samples (Table 1), the nanocomposite filaments exhibited significantly higher crystallinity and heat of fusion compared to the neat nylon control.

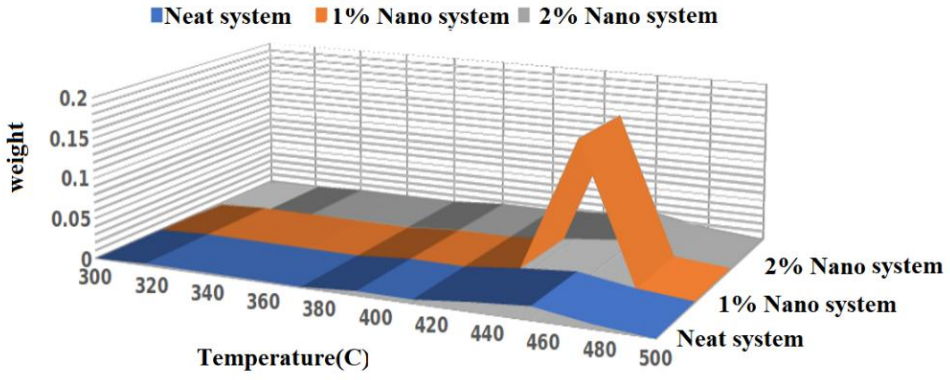

(a).

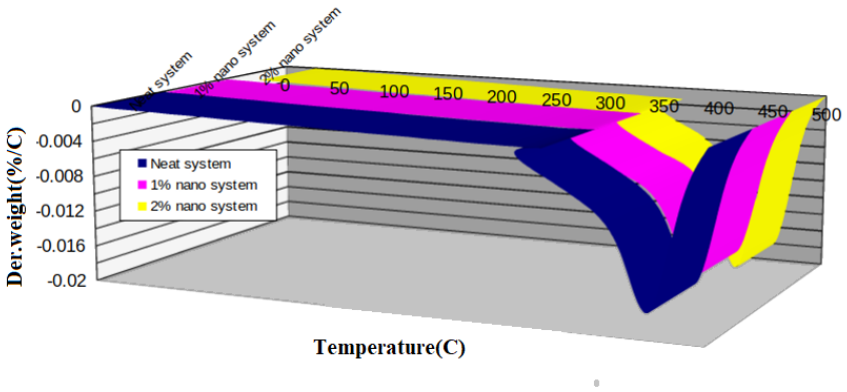

(b).

Figure 4. Thermogravimetric Analysis (TGA) Curves for neat nylon and nanocomposite filaments (a, b).

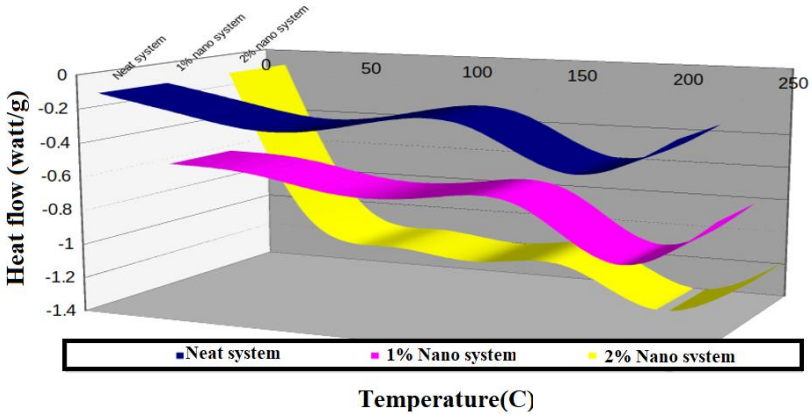

(a).

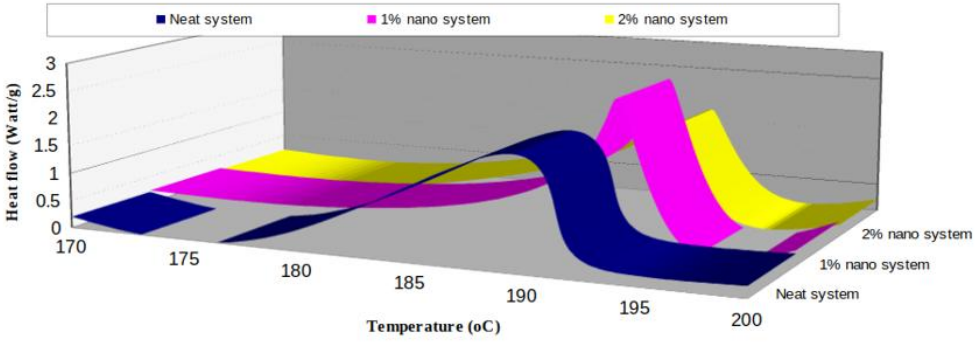

(b).

Figure 5. DSC curves for neat nylon and nanocomposite filaments (a, b).

Table 1. Differential scanning calorimetry.

Samples	T_g (°C)	T_m (°C)	H_f (Joule/g)	Crystallinity (%)
Neat nylon	49	224	52.24	24
1%ZnO–nylon	55	222	62.15	27
2%ZnO–nylon	56	223	64.2	28

Stress–strain diagrams

Tensile stress-strain (TSS) curves for neat nylon and the nylon nanocomposites are shown in Figures 5-7. Both materials exhibit nonlinear stress-strain behavior, including strain hardening, even before yielding. Table 2 summarizes the tensile properties under the various test conditions.

The stress-strain behavior of the materials is presented in Figures 6-8. For all materials tested, modulus increased with increasing strain rate. The parallel curves in the strain hardening region indicated that the hardening modulus is relatively insensitive to strain rate within the tested range.

At a strain rate of 2 min^{-1}, the 2 wt% ZnO nanocomposite shows superior mechanical performance compared to neat nylon, exhibiting a 23.4% increase in tensile modulus (Figure 9). While ZnONP incorporation significantly improves nylon mechanical properties, its impact on ductility is minimal, with comparable strain at break observed across all samples.

Sensitivity of strain rate

Neat nylon and its nanocomposites both display strain rate-dependent mechanical behavior, as shown in Table 2 and Figures 5-7. This characteristic is often described as strain rate sensitivity. Figure 10 shows how tensile properties vary with strain rate. The linear relationship between strength and ln ($\dot{\varepsilon}$) suggests power-law dependence. The slopes of these linear fits quantify the strain rate sensitivity of each material. The following equations describe the observed correlations between yield strength, tensile strength, and strain rate.

$$\sigma_b = \sigma_{b0}\left(1 + \lambda_1 \ln\frac{\dot{\varepsilon}}{\dot{\varepsilon}_b}\right) \quad (1)$$

$$\sigma_Y = \sigma_{Y0}\left(1 + \lambda_2 \ln\frac{\dot{\varepsilon}}{\dot{\varepsilon}_b}\right) \quad (2)$$

In Equations (1) and (2), σ_{b0} and σ_{Y0} represent the tensile strength and yield strength, respectively, at a reference strain rate, $\dot{\varepsilon}_0$. The coefficients λ_1 and λ_2 (defined in Equation (3)) quantify the strain rate sensitivity of each material.

$$\lambda_{12} = \frac{\partial(\sigma_b, \sigma_Y)}{\partial \ln \dot{\varepsilon}} \quad (3)$$

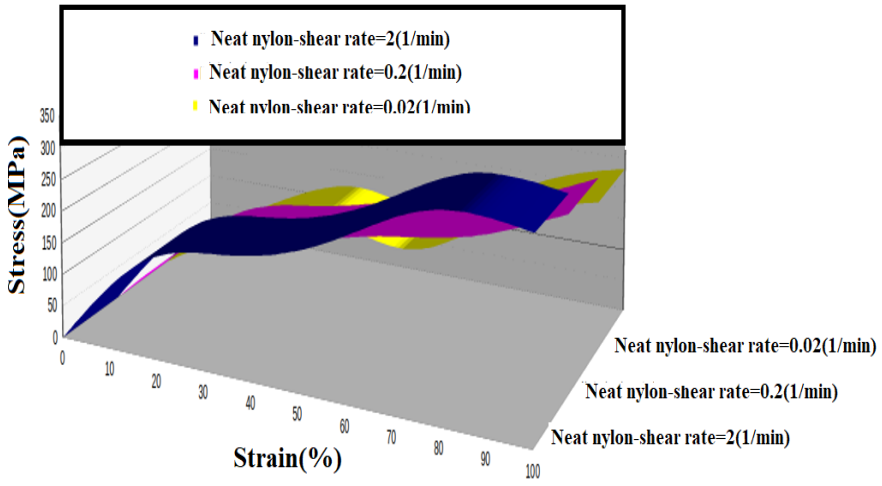

Figure 6. TSS curves for neat nylon at various strain rates.

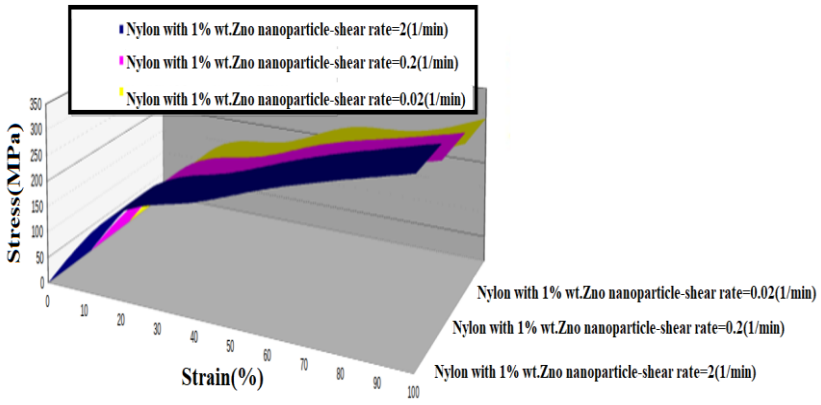

Figure 7. TSS curves for one wt.% ZnO/nylon Composite at various strain Rates.

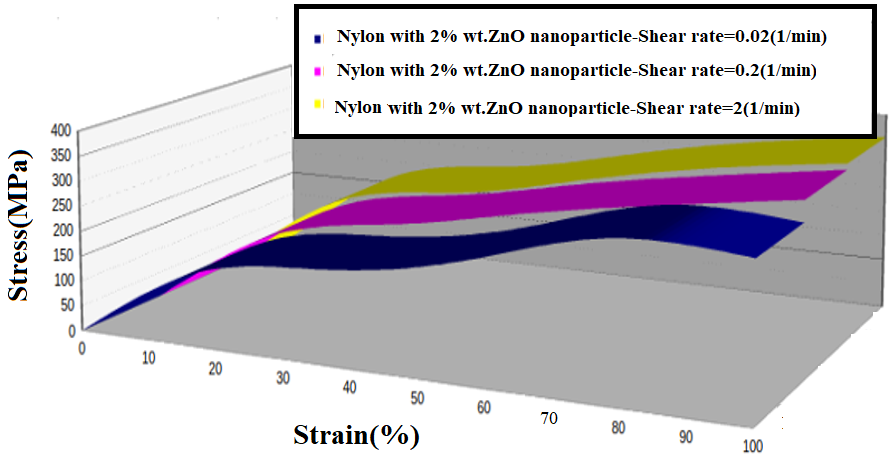

Figure 8. TSS curves for two wt. % ZnO/nylon composite at various strain rates.

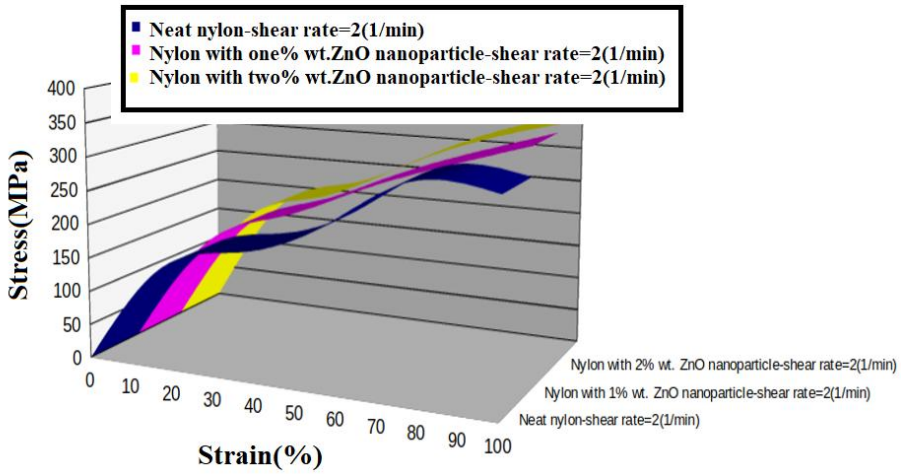

Figure 9. TSS curves for neat nylon and nanocomposite filaments.

Table 2. Mechanical characteristics of neat nylon and nanocomposites.

Material	Strain rate (1/min)	*E* (GPa)	σ_Y (MPa)	Hardening modulus (MPa)	UTS (MPa)
Neat Nylon	0.02	1.30	68.4	174	243
Neat Nylon	0.2	1.47	83.4	177	262
Neat Nylon	2	1.76	125	176	293
Nylon with 1 wt.% ZnO	0.02	1.65	96.7	206	287
Nylon with 1 wt.% nanoparticle	0.2	1.88	117	205	309
Nylon with 1 wt.% ZnO	2	2.08	129	204	311
Nylon with 2 wt.% ZnO	0.02	1.88	120	219	306
Nylon with 2 wt.% ZnO	0.2	1.95	125	215	313
Nylon with 2 wt.% ZnO	2	2.16	138	219	342

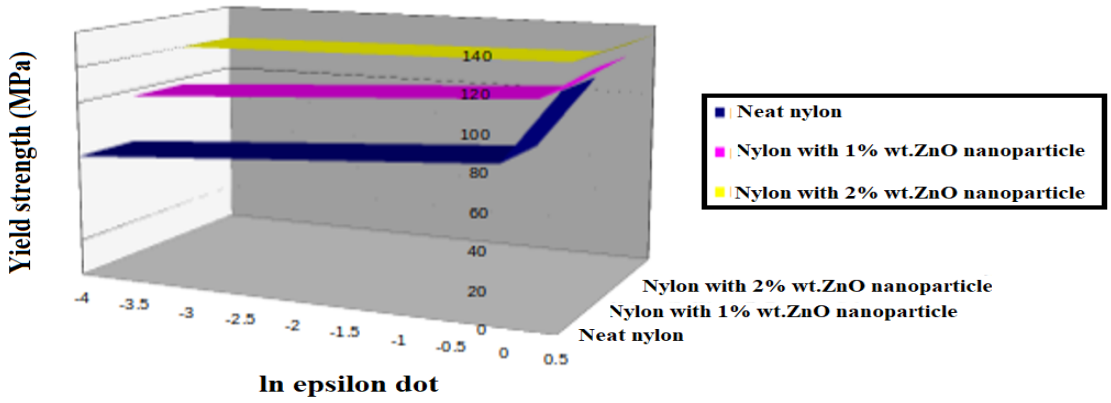

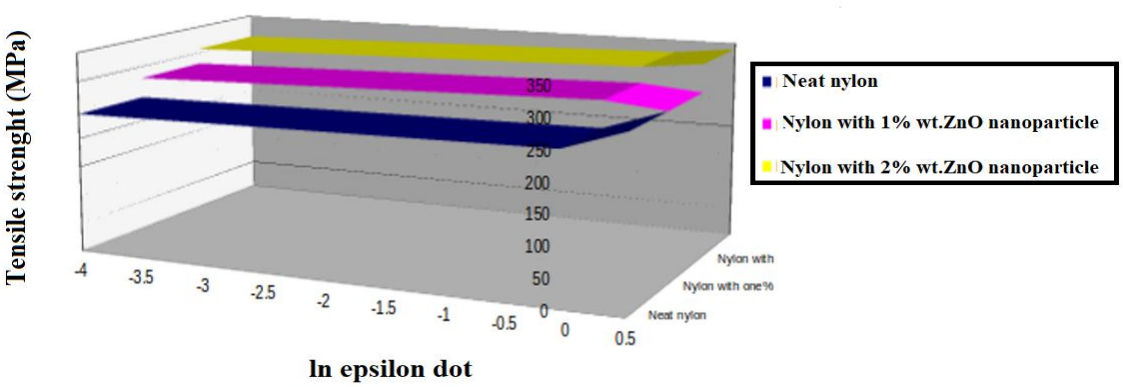

Figure 10. Yield and tensile strength variation with strain rate (ln ˙ε).

Least-squares regression analysis of the experimental data yielded the strain rate strengthening coefficients, λ_1 and λ_2, which are presented in Table 3. These results suggest that nanoparticles restrict polymer chain mobility at higher strain rates (Equation 4).

$$V = \frac{RT}{\lambda_2} \quad (4)$$

Activation volumes (ΔV), which reflect the energy barrier to atomic-level deformation, were calculated using Equation (4) and incorporating the gas constant (R), absolute temperature (T), and the strain rate sensitivity coefficient (λ). These calculated values for both neat nylon and the nanocomposites are presented in Table 3.

As shown, Figure 11 evaluates the effect of nanoparticle content and degree of tension on the viscosity coefficient. In Equation (5), E1 and E2 represent the elastic modulus of the spring in the Maxwell element and the spring in the Kelvin element, respectively, while η is the viscosity coefficient (stress × time). The initial slope of the stress-strain curve can be expressed as shown in Equations (6) and (7).

$$\sigma = \frac{E_1 E_2}{E_1 + E_2}\varepsilon + \frac{E_1^2 \dot{\varepsilon}\eta}{(E_1 + E_2)^2}\left[1 - \frac{E_1 + E_2}{\varepsilon}\frac{\varepsilon}{\dot{\varepsilon}}\right] \quad (5)$$

$$\frac{d\sigma}{d\varepsilon} = E_1 \quad (6)$$

$$\frac{d\sigma}{d\varepsilon} = \frac{E_1 E_2}{E_1 + E_2} \quad (7)$$

The viscosity coefficient relationships for pure nylon and nylon containing 1 and 2 weight percent nanoparticles are presented in Table 4.

XRD patterns of ZnONPs were obtained using a Miniflex XRD machine (Rigaku, Japan). The crystalline domain dimension (D) was calculated using Scherrer's equation:

$$D = K\lambda/\beta cos\theta$$

where ʎ represents the wavelength of the incident X-ray beam, θ is Bragg's diffraction angle, β is the width of the X-ray pattern line at half-peak height in radians, and the dimensionless shape factor (K) has a normal value of 0.89 but varies depending on the actual crystalline structure. SEM (FEI Company, USA) was used to study the morphology of the materials.

Density of nanocomposites

The theoretical density (ρth) of the nanocomposites is given by:

$$\rho_{th} = \rho_f V_f + \rho_m V_m$$

Where pf and pm are the density of Zno and matrix, respectively. V_f and V_m represent the volume fractions

of ZnO and matrix, respectively. The experimental density (ρex) was calculated using Archimedes' principle and following eq.:

$$P_{ex} = {W_{air} p_{liq}}/{W_{air} - W_{liq}}$$

W_{liq} and W_{air} are the weights of samples in liquid medium (ethanol) and air, respectively.

Thermal conductivity test

A Lee's Disc device (George and Griffin™) can be used to calculate the thermal conductivity coefficients of test materials. In this device, heat flows from the heater into each sequentially stacked disc. The temperatures of the three discs (TA, TB, and TC) are determined using internally inserted thermometers. The sample (S) is placed between the discs A and B, while the heater is placed between discs B and C. It is essential to ensure that the surfaces of the copper are clean and in good contact to obtain the best heat transfer. The thermal conductivity value is determined using the following equation:

$$K\left(\frac{T_B - T_A}{d_s}\right) = e\{T_A + \frac{2}{r}\left(d_A + \frac{1}{4}d_s\right)T_A + \frac{1}{2r}d_s T_B\}$$

(8)

Where e denotes the amount of thermal energy that passes through the unit area of the disc material per second ($W/m^2.k$), and it is estimated from the following equation:

$$IV = \pi r^2 e(T_A + T_B) + 2\pi r e d_A T_A + d_s \frac{1}{2}(T_A + T_B) + d_B T_B + d_C$$

(9)

IV is the thermal energy that passes through the heating coil per unit time; TA, T B, and TC represent the respective disc temperatures; and d and r are the thickness and radius of the disc (mm), respectively. According to ASTM-D150, the specifications for measuring thermal conductivity were a thickness of 6.73 mm and a diameter of 40 mm.

Dielectric property

The device used for measuring the dielectric constant values of the composites was an electrical circuit (connected in series) consisting of a capacitor, a resistor, a coil, a frequency generator, and an ammeter. After placing the sample between the capacitor's plates, the frequency of the power supplier was adjusted until the maximum current value was obtained. The frequency, which reflects the resonance frequency value (fr), was recorded at this maximum value. The fr value was then calculated without a sample (i.e., in the presence of air only). From the relationship, the capacitor's capacity could be determined as: $C = {1}/{4\pi^2 f_r^2 L}$ where L represents the inductance of the coil. The dielectric constant (εr) can be calculated from the equation, $\varepsilon_r = {C}/{C_0}$ in which Co represents the capacity of the capacitor in the existence of air, while C represents the capacity of the capacitor in the presence of a sample. (See Table.5)

Table 3. Model variables for neat nylon and nanocomposites.

Material	**λ1**	**λ2**	***V* (nm)3**	**η, shear rate=2 (1/min)**	**η, shear rate=0.2 (1/min)**	**η, shear rate=0.02 (1/min)**
Nylon	10.7	12.4	12.4	80	550	4000
One wt.% ZnO	9.12	7.91	7.91	85	700	6000
One wt.% ZnO	7.82	3.78	3.78	90	800	7000

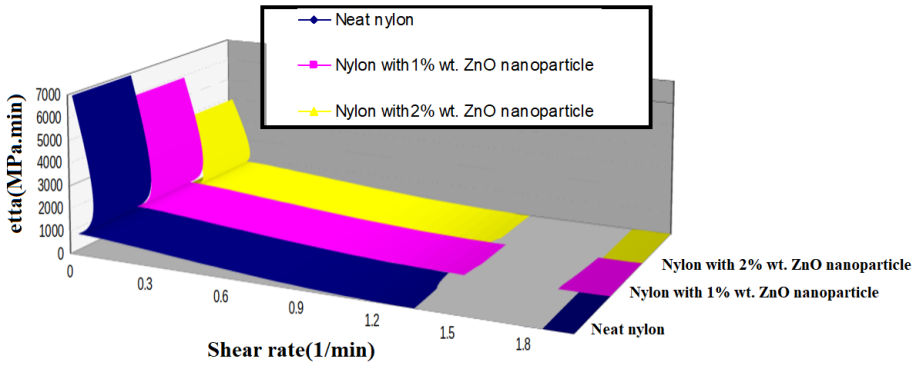

Figure 11. The effect of nanoparticle content and degree of tension on the viscosity coefficient, η.

Table 4. Viscosity coefficient relationships for pure nylon and nylon containing 1 and 2 weight percent nanoparticle

Nylon	$\eta = 143\ \dot{\varepsilon}^{.=0.849}$ (MPa×min)
Nylon containing 1% by weight of nanoparticles	$\eta = 160\ \dot{\varepsilon}^{.=0.924}$ (MPa×min)
Nylon containing 2% by weight of nanoparticles	$\eta = 173\ \dot{\varepsilon}^{.=0.945}$ (MPa×min)

Table5: Experimental values of dielectric constant, resistivity, thermal conductivity of nanocomposites, diffusivity and density of all samples.

Samples	**Dielectric constant**	**Resistivity (Ω.m)*10^{-11}**	**Thermal conductivity of nanocomposites (w/m.C)**	**Diffusivity (w/m^2.C)**	**Density (mg/cm)**
Neat nylon	2.6	3.8	0.31	6.41	1.395
1%ZnO–nylon	4.3	3.3	0.48	6.05	1.409
2%ZnO–nylon	5.4	1.9	0.46	5.78	1.415

CONCLUSION

This study examined the effects of ZnONP incorporation on nylon filament properties, with the following key findings: (1) both neat nylon and the nanocomposites exhibited strain rate-dependent mechanical behavior. (2) The nanocomposites showed significant improvements in mechanical properties compared to neat nylon, while maintaining similar failure strains. (3) DSC and TGA revealed enhanced thermal stability in the nanocomposites, evidenced by increased decomposition and glass transition

temperatures, with no change in melting temperature. (4) A nonlinear constitutive model was developed to quantify the observed strain rate sensitivity, with simulations suggesting a decrease in the viscosity coefficient (η) with increasing strain rate. Nanoparticle incorporation appeared to increase the nylon matrix viscosity, potentially impacting high-strain-rate behavior. The 2% ZnONP sample exhibited higher density and fewer free spaces compared to the 1% ZnONP sample, which showed relative weakness and random masses potentially due to weak Van der Waals forces between the matrix and NPs. Characterization confirmed the smooth, spherical form and hexagonal wurtzite structure of the ZnONPs. Finally, the 2% ZnONP sample demonstrated the highest dielectric constant, a 65% increase compared to neat nylon.

Application of nanocomposites in real-world engineering problems

Nylon 6 nanocomposites offer a range of potential applications across various industries due to their enhanced properties. In the automotive sector, their light weight (resulting from increased strength and stiffness allowing for thinner parts) contributes to improved fuel efficiency and reduced emissions. Enhanced durability and noise reduction are additional benefits. Aerospace applications benefit from the reduced weight of nylon 6 nanocomposites, crucial for fuel-efficient aircraft components, and their improved performance due to high strength-to-weight ratio and fatigue resistance. Electronics and electrical applications can leverage the improved insulation, heat dissipation, and flame retardancy offered by these materials. Packaging applications can benefit from enhanced barrier properties, extending shelf life, and increased strength and durability, reducing damage during transport. Finally, in the biomedical field, with appropriate surface modifications, nylon 6 nanocomposites offer biocompatibility and enhanced mechanical properties suitable for applications like orthopedic implants, drug delivery systems, and tissue engineering scaffolds. These examples highlight the potential of nylon 6 nanocomposites to address real-world engineering challenges, and continued research promises further innovative applications with significant societal and economic impact.

REFERENCES

[1]. Wang Shuyu, Duan Shuaiyang, Yang Tianyu, Zhonghai He, Xia Zhichao, Zhao Yuliang, A self-powered strain sensor utilizing hydrogel-nanosheet composites, Zn foil, and silver-coated nylon, Sensors and Actuators A: Physical, Volume 364, 1 December 2023, 114824.

[2]. Rana Kiran, Jassal Manjeet, Agrawal Ashwini K., Solution spun electrically conductive nylon 6/poly(pyrrole) nanotubes-based composite fibers, Synthetic Metals, Volume 303, April 2024, 117550.

[3]. Gavande Vishal, Nagappan Saravanan, Seo Bongkuk, Cho Young-Seok, Lee Won-Ki, Transparent nylon 6 nanofibers-reinforced epoxy matrix composites with superior mechanical and thermal properties, Polymer Testing, Volume 122, May 2023, 108002.

[4]. Yilmaz Musa, Ekrem Mürsel, Avci Ahmet, Impact resistance of composite to aluminum single lap joints reinforced with graphene doped nylon 6.6 nanofibers, International Journal of Adhesion and Adhesives, Volume 128, January 2024, 103565.

[5]. Atir Salman, S. Ali Hasan, Nimra S.Sadia, Zhao Tingkai, Shakir HM Fayzan, Rehan ZA, Achieving enhanced EMI shielding with novel non-woven fabric using nylon fiber coated with polyaniline via in situ polymerization, Synthetic Metals, Volume 293, March 2023, 117250.

[6]. Mishra Kushal, Singh Aparna, Effect of graphene nano-platelets coating on carbon fibers on the hygrothermal ageing driven degradation of carbon-fiber epoxy laminates, Composites Part B:

Engineering, Volume 269, 15 January 2024, 111106.

[7]. Zeynali Yasaman, Niroumand Hamed, Ziaie Moayed Reza, Stabilizing cohesive soils with Micro- and Nano- fly ash as Eco-friendly Materials: An experimental study, Construction and Building Materials, Volume 399, 5 October 2023, 132490.

[8]. Hazarika Ankita, Deka Biplab K., Park Hyunmin, Hwang Yun Jae,Jaiswal Anand P., Park Young-Bin, Park Hyung Wook, Hierarchically designed 3-D printed porous nylon fabric-based personal thermoregulatory for radiative and directional wick-evaporative cooling, Chemical Engineering Journal, Volume 471, 1 September 2023, 144536.

[9]. Liu Kan, Su Yishi, Wang Xiaozhen, Cai Yunpeng, Cao He, Ouyang Qiubao, Zhang Di, Achieving simultaneous enhancement of strength and ductility in Al matrix composites by employing the synergetic strengthening effect of micro- and nano-SiCps, Composites Part B: Engineering, Volume 248, 1 January 2023, 110350.

[10]. Liu Yan-Jun, Yang He-Yun, Hu Yan-Yun, Li Zheng-Hao, Yin Hao, He Yun-Tian, Zhong Keng-Qiang, Yuan Li, Zheng Xing, Sheng Guo-Ping, Face mask derived micro(nano)plastics and organic compounds potentially induce threat to aquatic ecosystem security revealed by toxicogenomics-based assay, Water Research, Volume 242, 15 August 2023, 120251.

[11]. Lin Huiping, Kehinde Olonisakin, Lin Chengwei, Fei Mingen, Li Ran, Zhang Xinxiang, Yang Wenbin, Li Jian, Mechanically strong micro-nano fibrillated cellulose paper with improved barrier and water-resistant properties for replacing plastic, International Journal of Biological Macromolecules, Volume 263, Part 1, April 2024, 130102.

[12]. Dehghanian Zahra, Lajayer Behnam Asgari, Atigh Zahra Biglari Quchan, Nayeri Shahnoush, Ahmadabadi Mohammad, Taghipour Leila, Senapathi Venkatramanan, Astatkie Tess, Price G.W., Micro (nano) plastics uptake, toxicity and detoxification in plants: Challenges and prospects, Ecotoxicology and Environmental Safety, Volume 268, December 2023, 115676.

[13]. Cui Qian, Wang Feilong, Wang Xiaoxiao, Chen Tao, Guo Xuetao, Environmental toxicity and ecological effects of micro(nano)plastics: A huge challenge posed by biodegradability, TrAC Trends in Analytical Chemistry, Volume 164, July 2023, 117092.

[14]. Zhao Yonghuan, Meng Yang, Yu Pengxiang, Hu Xiaoxiao, Su Juanjuan, Han Jian, Modified reduced graphene oxide-LDH/WPU nanohybrid coated nylon 6 fabrics for durable photothermal conversion performance, Applied Surface Science, Volume 622, 15 June 2023, 156900.

[15]. Le Van-Giang, Nguyen Minh-Ky, Nguyen Hoang-Lam, Lin Chitsan, Hadi Mohammed, Hung Nguyen Tri Quang, Hoang Hong-Giang, Nguyen Khoi Nghia, Tran Huu-Tuan, Hou Deyi, Zhang Tao, Bolan Nanthi S., A comprehensive review of micro- and nano-plastics in the atmosphere: Occurrence, fate, toxicity, and strategies for risk reduction, Science of The Total Environment, Volume 904, 15 December 2023, 166649.